Selective p38α mitogen-activated protein kinase inhibitor attenuates lung inflammation and fibrosis in IL-13 transgenic mouse model of asthma

Jing Ying Ma[1]
Satyanarayana Medicherla[1]
Irene Kerr
Ruban Mangadu
Andrew A Protter
Linda S Higgins

[1]Scios Inc, Fremont, CA, USA
[1]Jing Ying Ma and Satyanarayana Medicherla contributed equally to this work

Abstract: p38 Mitogen-activated protein kinase (MAPK) plays a critical role in the activation of inflammatory cells. We investigated the anti-inflammatory effects of a p38α-selective MAPK inhibitor (SD-282) in a mouse transgenic (CC10:IL-13) asthma model. The CC-10-driven over-expression of IL-13 in the mouse lung/airway has been shown to result in a remarkable phenotype recatitulating many features of asthma and characterized by eosinophilic and mononuclear inflammation, with airway epithelial cell hypertrophy, mucus cell metaplasia, the hyperproduction of neutral and acidic mucus, the deposition of Charcot–Leyden-like crystal, and airway sub-epitheilial fibrosis. Here we show how activated p38 MAPK can be observed in the lungs at the onset of asthma ie, around 8 weeks of age in both female and male mice. We also show that administration of a p38α MAPK selective inhibitor, SD-282 at 30 or 90 mg/kg, twice a day for a period of four weeks beginning at the onset of asthma, significantly reduced the inflammation ($p < 0.001$); hyperplasia of airway epithelium ($p < 0.05$); goblet cell metaplasia and mucus hypersecretion ($p < 0.001$) and reduced lung remodeling and fibrosis ($p < 0.01$), alleviating the severity of lung damage as measured by a composite score ($p < 0.05$). Furthermore, SD-282 significantly reduced activated p38 MAPK in the lymphocytes and epithelial cells ($p < 0.001$). Simultaneously, identical studies were conducted with an anti-fibrotic TGFβR1 kinase inhibitor (SD-208) which demonstrated anti-fibrotic but not anti-inflammatory properties. These findings suggest that the p38α-selective MAPK inhibitor may have dual therapeutic potential in attenuating both the inflammatory component and the fibrotic component of asthma and other Th2-polarized inflammatory lung diseases.

Keywords: inflammation, asthma, fibrosis, p38α-selective MAPK inhibitor, SD-282, phosphorylated p38 MAPK, TGFβ inhibitor, SD-208, phosphorylated SMAD2/3

Introduction

In the family of mitogen-activated protein kinases (MAPK), three major enzymes have been well characterized, including the extracellular signal-regulated kinase (ERK or p42/44MAPK), the c-Jun NH2-terminated kinase, and the p38 MAPK (Sugden et al 1998). p38 MAPK, a serine-threonine kinase, is activated in response to a variety of environmental stimuli, including inflammation and cellular stress (Underwood et al 2000). Four p38 MAPK isoforms, including α, β, δ, and γ have been characterized. In the human lung cDNA libraries, the levels of α and β transcripts are higher than those of δ and γ (Jiang et al 1997). Hence it is worth pursuing the pharmacology of an α-selective p38 MAPK inhibitor to keep the p38 MAPK-based drug hunt active.

IL-13 is a pleiotropic cytokine produced largely by activated CD4+ Th2 lymphocytes. The CC10-driven over-expression of IL-13 in the lung/airway in CC10:IL-13 transgenic (Tg (+)) mice causes a profound phenotype reminiscent of asthma in humans, characterized by eosinophilic and mononuclear inflammation, with

Correspondence: Jing Ying Ma
PRD, La Jolla, Johnson & Johnson, 3210 Merryfield Row, San Diego, CA 92121, USA
Tel +1 858 450 2033
Email jma2@its.jnj.com

mucus hyperproduction, epithelial metaplasia, subepithelial fibrosis, airway obstruction and AHR (Zhou et al 1999). The role and activity of p38 MAPK in the Tg (+) mouse model of asthma is not well understood.

It has been demonstrated that p38 MAPK may play an important role in asthma and other inflammatory lung diseases. A recent study revealed that the p38 MAPK inhibitor SB239063 markedly reduced ovalbumin-induced pulmonary eosinophilia in animal models of asthma (Underwood et al 2000). However SB239063 is not selective between p38α and p38β MAPK isoforms. In addition, the airway eosinophilia was the only endpoint reported in that study. The efficacy of p38α-selective inhibitor SD-282 in a model of allergic airway remodeling and bronchial hyperresponsiveness was reported recently (Nath et al 2006). In the present study, we used p38α-selective inhibitor SD-282 and investigated its anti-inflammatory effects in a mouse transgenic asthma model. We tested both a low dose (30 mg/kg) and a high-dose (90 mg/kg) of SD-282. SD-282 at 90 mg/kg (twice/day, orally) significantly reduced IL-13-induced increases in infiltrating inflammatory cells, lymphocytes, macrophages, p38 MAPK activation, and IL-1β expression. It also inhibited IL13-induced airway mucus production, epithelial cell hypertrophy and, intriguingly, lung fibrosis.

Historical data suggests that transforming growth factor-beta receptor type 1 (TGFβRI) kinase activity, but not p38 MAPK activation, is required for TGFβRI-induced fibrosis (Kapoun et al 2006). Further, TGFβRI not only signals through SMAD2/3 but also through MAPK. Interestingly, both phosphorylated, and thereby activated p38 MAPK and SMAD2/3, are present in Tg (+) mice. Therefore we also investigated the effect of TGF-β receptor I kinase inhibitor, SD-208 at both a low dose and a high-dose on lung fibrosis. SD-208 at a high-dose demonstrated efficacy selectively on fibrosis in this model. Our findings show that the use of the p38α-selective MAPK inhibitor, but not TGFβR1K kinase inhibitor, has effective dual roles in attenuating pulmonary disorders including inflammation and fibrosis, and suggest that the p38α-selective MAPK inhibitor may have therapeutic potential for asthma and other inflammatory lung diseases.

Materials and methods

Chemical descriptions

Both p38α-selective MAPK and TGFβRI kinase inhibitors SD-282 and SD-208 were synthesized by the Medicinal Chemistry Department at Scios, Inc. Chemical structures and descriptions were reported in our earlier communication (Kapoun et al 2006).

SD-282 potency and specificity

IC_{50} of SD-282 against the human p38 MAPKs (α, β, γ, and δ isoforms) were performed and reported in our earlier communication (Medicherla et al 2006). The IC_{50} values of SD-282 for p38α MAPK were derived from two studies. As reported previously (Medicherla et al 2006; Sweitzer et al 2004), SD-282 demonstrates 14.3-fold selectivity for p38α MAPK (IC_{50} values of 0.0016 and 0.0011 μM) compared with p38β MAPK (IC_{50} values of 0.023 and 0.022 μM), whereas inhibition of p38γ MAPK and p38δ MAPK was less than 50%, even at concentrations of 10 μM. When tested in vitro at a concentration of 10 μM, SD-282 demonstrated no inhibitory activity against a panel of other kinases, including extracellular signal-regulated kinase 2, c-Jun NH_2-terminal kinase-1, and mitogen-activated protein kinase-activated protein kinase-2. In addition, SD-282 demonstrates no effect on the activity of purified COX-1 or COX-2 enzymes.

Pharmacokinetics studies in IL-13 mice revealed that SD-282 and SD-208 at 90 mg/kg reached peak levels 30 min after their administration, and their trough levels at that dose are trace amounts at 8 h. Hence, mice in the studies reported here were treated twice daily by oral gavage with SD-282 and SD-208.

Animals

CC10:IL-13 transgenic mice, used as Tg (+), were provided by Dr Jack A Elias (Yale University of Medicine) and wild type mice were provided by Charles River Laboratories, San Diego, CA. The techniques for identifying transgenic mice were obtained from Dr Elias's Laboratories (Tang et al 1996; Pack et al 1981; Ray et al 1997). Transgenic mice were generated in (CBA × C57BL/6) F2 eggs using a standard pronuclear injection as described previously (Ray et al 1997; Hogan et al 1986). The presence or absence of the transgene in the resulting mice and their progeny was determined using tail DNA and Southern blot analysis with ^{32}P-labeled murine IL-13 cDNA as a probe or PCR. When PCR was used, primers were used to span the IL-13–hGH junction that was unique to the transgene. The primers were: 5'-CAA AAC TGC TCA GCT ACA CAA AG-3' and 5'-GAG CTG TTT GTT TTT CTC TCT CC-3'. The following PCR protocol was used: 95 °C for 8 min; 35 cycles of 95 °C for 1 min, 56 °C for 1 min, and 72 °C for 1 min, and a final extension at 72 °C for 10 min (Zhou et al 1999).

Measurement of activated p38 MAPK in the lungs of CC10:IL-13 transgenic Tg (+) mice

Animal experimental protocols were approved by the Preclinical Ethical Committee of Charles River, San Diego, US. Phosphorylated p38 MAPK was measured in both male and female mice at time intervals including 4, 8, and 12 weeks. Three mice per time point were taken for histochemical analysis of posphorylated p38 MAPK and phosphorylated SMAD2/3. Details for immunohistochemistry are provided in a later section.

Experimental design

Grouping was randomized and animals were divided into seven groups. In each group were ten mice (5 females and 5 males). Baseline Tg (+) mice were sacrificed at 8 weeks (±3days) of age (n = 8). At the age of 8 weeks treatment was initiated in remaining groups (n = 10). Mice were administered p38α-selective MAPK inihbitor SD-282 via gastric gavage at doses of 30 (low dose) and 90 mg/kg (high-dose) respectively, twice daily for 4 weeks, or TGFbetaRI inhibitor SD-208 at 20 (low dose) and 60 mg/kg (high-dose) twice daily, or 1% methyl cellulose vehicle. Tg (+) mice in the test compound or vehicle-treated groups were sacrificed at the age of 12 weeks. Wild type mice without treatment were sacrificed at 12 weeks and used as Tg (–) naïve.

Histology, immunohistochemistry, and morphometry

Left lungs were inflated with 10% buffered formalin and fixed in the same fixative for 48 hours. Three equal slabs from each left lung were segmented transversely so that the first generation of bronchus (segmental bronchus) was obtained in cross section, and samples were processed and paraffin embedded. Serial sections were cut at 5 μm thickness and stained with hematoxylin and eosin (H&E), periodic acid-schiff and hematoxylin (PASH), Alcin blue or Masson's trichrome stains.

For immunohistochemical (IHC) staining, slides were deparaffinized and hydrated in PBS followed by blocking the endogenous peroxide with 3% hydrogen peroxide. To avoid nonspecific reaction with the primary antibody, slides were pretreated with 10% normal donkey serum before incubation with the primary antibody produced in goat, with 10% normal goat serum before incubation with primary antibody produced in rat and rabbit. The primary antibodies used in this study were goat anti-CD3 at concentration of 1:100 (Santa Cruz Biotechnology, Inc. Cat. No. sc-1127), goat anti-mouse IL-1β at concentration of 1:100 (R&D System, Cat. No. AF-401-NA), rat anti-mouse F4/80 at concentration of 1:25 (Novus Biological, Cat. No. AB 6640–250), rabbit anti-phospho-p38 MAPK (Thr180/Tyr182) at concentration of 1:50 (Cell Signaling, Cat. No. 4634), rabbit anti-phospho-SMAD2/3 at concentration of 1:5000. (Cell Signaling, Cat. No. 3101L). Normal goat IgG, normal rat IgG, and normal rabbit IgG were used as negative controls for the primary antibody produced in goat, rat, and rabbit respectively. Donkey anti-goat biotinlated IgG (Chemicon International, Inc. Cat. No. AP180B) for CD3 and IL-1β, goat anti-rat biotinlated IgG (Chemicon International, Inc. Cat. No. AP183B) for F4/80, and goat anti-rabbit biotinlated IgG (Chemicon International, Inc. Cat. No. AP187B) for p38 MAPK and SMAD2/3 were used as secondary antibodies. The immunoreactivities were visualized by ABC reagents (Vector, Burlingame, Cat. No. PK-6100) and diaminobenzidine (Research Genetic, Cat. No. 750118) followed by counterstaining with hematoxylin.

Histological and morphometric analysis

The development of asthma based on histological parameters (Hogan et al 1986; Gupta et al 1998; Zhou et al 1999) was evaluated quantitatively following H&E stain to demonstrate the presence of inflammation, PASH stain to demonstrate the bronchial epithelium, and mucin within goblet cell and trichrome stain to demonstrate the muscular layer and the presence of extracellular matrix. The histological parameters presented included inflammation and crystal formation, hyperplasia of bronchial epithelium, goblet cell metaplasia and mucus hypersecretion, smooth muscle hypertrophy and hyperplasia, subepithelial fibrosis in airway wall, and fibrosis of lung parenchyma. Morphometric (Image) analysis was performed using a Nikon E800 light microscope equipped with Q Imaging digital camera. Image Pro Plus 4.5 software (Media Cybernetics, Silver Spring, MD) was used for quantitative measurements. The total area of lungs from the three slabs of left lung and inflamed lung area were measured. The percentage of inflamed lung area was then calculated, to evaluate inflammation. The inflamed area was defined as different inflammatory cell infiltration and the deposition of Charcot–Leyden-like crystal. The inflammatory cells included eosinophils, neutrophils, macrophages, plasma cells, and lymphocytes. The area was measured manually using the area measurement feature of Image Pro Plus 4.5 software. Both total area and inflamed

area were measured throughout the lung section. Sections stained with H&E were used to measure inflammation under a 10x lens. The thickness of epithelial cells in the segmental bronchus was measured, to evaluate hyperplasia of the bronchial epithelium. The thickness of the epithelium was measured by the height (Figure 3b, marked by I), a line drawn perpendicular to the basal lamina underlying the surface of epithelium. The height of the epithelium from four zones of segmental bronchus, at 12, 3, 6, and 9 o'clock (Figure 4b–C) per section was measured using the length measurement feature of Image Pro Plus 4.5 software. The average height from the four zones was calculated. Sections stained with PASH were used to measure the thickness of the epithelium under a 40x lens. The thickness of the muscular layer in the segmental bronchus was measured, to evaluate muscle hypertrophy and hyperplasia. The thickness of the muscular layer was measured by the height, a line drawn perpendicular to the basement membrane underlying the muscular layer. The height of the muscular layer from four zones of segmental bronchus, at 12, 3, 6, and 9 o'clock (Figure 5c–A) per section was measured using the length measurement feature of Image Pro Plus 4.5 software. The average height from the four zones was calculated. Sections stained with Masson's trichrome were used to measure the thickness of the muscular layer under a 40x lens. The percentage of mucin-secreted goblet cells in the segmental bronchus was counted to evaluate the goblet cell metaplasia and mucus hypersecretion. Total epithelial cells and PASH-stained mucin-positive goblet cells in the segmental bronchus were counted manually under a 40x lens. The percentage of mucin-secreted goblet cells was then calculated. The thickness of basement membrane was measured to evaluate subepithelial fibrosis, and the total area (mm^2) of collagen deposition per section was measured to evaluate lung fibrosis. The thickness of basement membrane measurement was similar to the measurement of the muscular layer. The total areas (mm^2) of collagen deposition per section were measured using Image Pro Plus 4.5 software. Collagens stained (with Masson's trichrome) in blue were chosen as the area of interest, and the threshold was set up to select the blue area. The total number of blue areas per section under 10x were selected and measured. Then the total collagen depositions were calculated to evaluate lung fibrosis.

The severity of the lung damage was obtained from the total scores of histological parameters. Scores were obtained from the qualitative analysis of each parameter defined as normal = 0, mild = 1, moderate = 2, severe = 3, and very severe = 4.

Immunohistochemical and morphometric analysis

Phospho-p38 MAPK and IL-1β IHC staining was analyzed qualitatively for the presence of positive labeling and the intensity of staining on a score of 0 to 4, none = 0, mild = 1, moderate = 2, strong = 3, and strongest = 4. For CD3 and F4/80 IHC, the CD3 positively labeled T-lymphocytes and F4/80 positively labeled macrophages in 10 independent hot fields under a magnification of 400 (40 × lens) were each counted. P-SMAD2/3 staining was analyzed quantitatively by: the percentage of positively labeled epithelial cells in the airway wall; the percentage of positively labeled proliferate alveolar epithelial cells (type-2); macrophages and fibroblasts in the lung parenchyma in 10 independent hot fields under a magnification of 400 (40× lens).

Statistical analysis

Data were analyzed by one-way ANOVA followed by the Bonferroni multiple group comparison test. A p value < 0.05 was accepted as statistically significant.

Results

First, presence and the temporal and spatial pattern of activation of p38α MAPK and of TGFβRIK were determined in the CC10:IL-13 tg lung. Next, the effects of p38 MAPK and TGFbRIK inhibition on the development of asthma were evaluated by measuring the different histological parameters and the severity of lung damage. SD-282 at 90 mg/kg, BID for 4 weeks did not cause any weight loss or animal deaths.

Phosphorylated p38 MAPK and SMAD2/3 levels in the Tg (+) lung

Both p38 MAPK and SMAD2/3 were phosphorylated, indicating activation, in Tg (+) lung but the cellular pattern of these two effectors differed. Phospho-p38 (p-p38) MAPK was found in bronchial and bronchiolar epithelial cells and infiltrated lymphocytes (Figure 1a). A strong intensity of p-p38 MAPK staining was found in both 8- and 12-week-old Tg (+) mice. Mild intensity of p-p38 MAPK staining was found in 16 week-old Tg (+) mice. No p-p38 MAPK activation was found in either 8- or 12-week-old Tg (–) mice.

Phospho-SMAD2/3 (p-SMAD2/3) activation was found in epithelial cells in airway (Figure 1b) and lung parenchyma (Figure 1c) such as alveolar epithelial cells (mostly type 2), fibroblasts, and macrophages. p-SMAD2/3 activation was found in 29% of epithelial cells in the airway with moderate

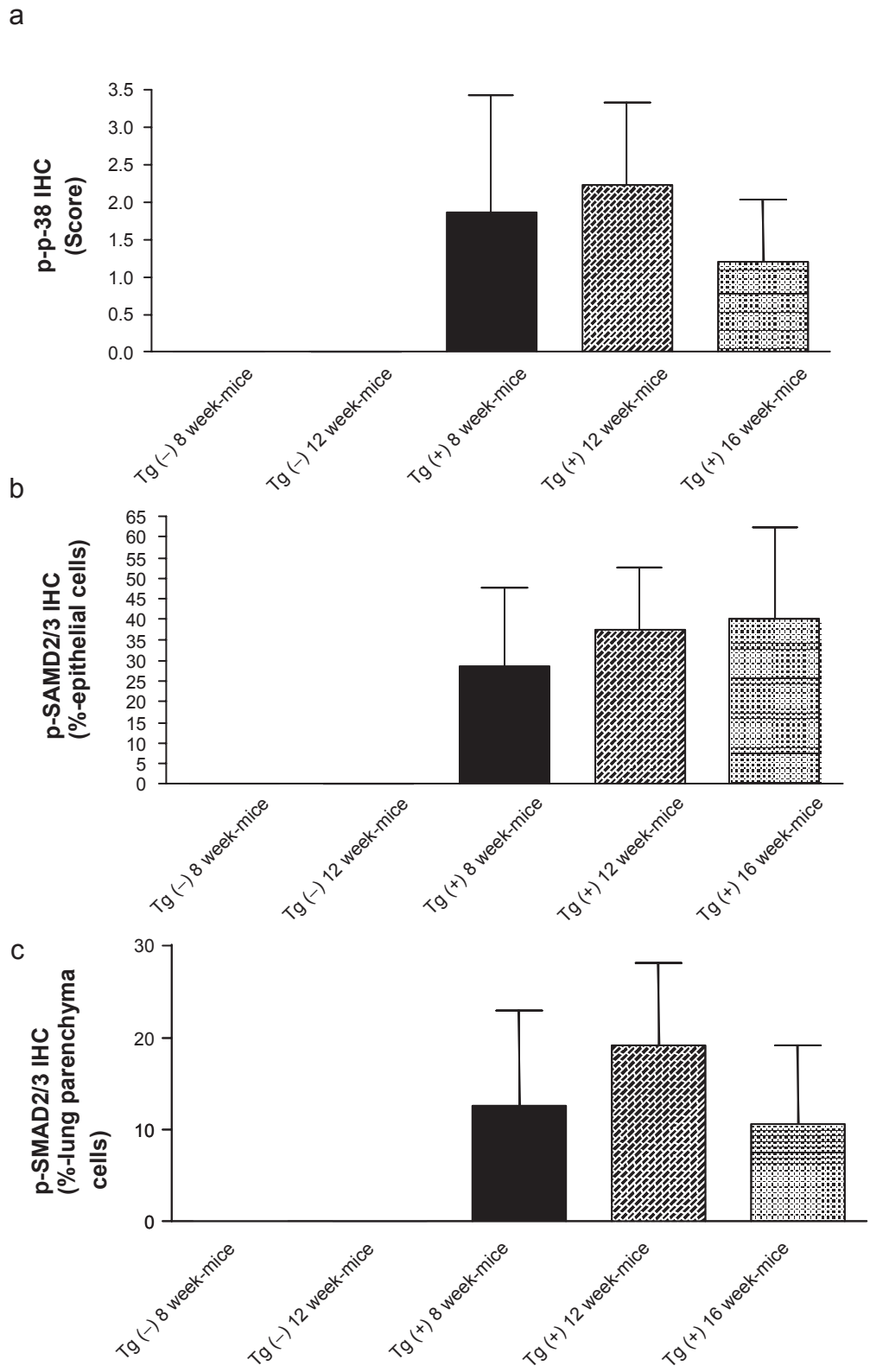

Figure 1 p38 MAPK and SMAD 2/3 phosphorylation in lungs of CC10:IL-13 transgenic mice during development of asthma-like phenotype (8–16 weeks of age). The noted values represent the MEAN±SD, n = 3. **[a]** Score of p-p38 MAPK (IHC) activation in the epithelial cells of airway and infiltrated lymphocytes. **[b]** Percentage of p-SMAD2/3 (IHC) positively labeled epithelial cells in the airway. **[c]** Percentage of p-SMAD2/3 (IHC) positively labeled lung parenchyma cells.

intensity and 13% in lung parenchyma in 8-week-old Tg (+) mice. p-SMAD2/3 activation was found in 38% of epithelial cells in the airway with moderate intensity and 19% in lung parenchyma in 12-week-old Tg (+) mice. p-SMAD2/3 activation was found in more than 40% of epithelial cells in the airway with strongest intensity, and 11% in the lung parenchyma in 16-week-old Tg (+) mice. No p-SMAD2/3 activation was found in any of the cells in either 8 or 12-week-old Tg (–) mice.

SD-282 reduces inflammation, edema, and crystal formation in the lungs

In the Tg (+) vehicle-treated mice, the lungs were enlarged (edema) and consolidated. Alveoli, small airways, and large airways were filled with lymphocytes, eosinophils, neutrophils, and prominent numbers of enlarged macrophages which contained granular and crystalline intracellular materials (Figure 2a, 2b, and 2c). Alveoli and small and large airways were filled with Charcot–Leyden-like crystals (Hogan et al 1986); that is, long, thin, rectangular and needlelike crystals composed of amorphous proteinaceous material. These histological changes were mild in the mice in the Tg (+) baseline group. In the Tg (+) SD-282 high-dose group, the lungs were observed to be less consolidated, and alveoli and airways were filled with fewer eosinophils, lymphocytes, macrophages, and crystals. The total inflamed left lung area was 24.29 ± 16.88 mm^2 in the baseline group and 60.39 ± 12.56 mm^2 in the vehicle-treated group. In the SD-282 high-dose treated group, the inflamed left lung area was 38.84 ± 10.73 mm^2 and reduced 36% compared with the Tg (+) vehicle group ($p < 0.05$). Treatment with SD-282 at a

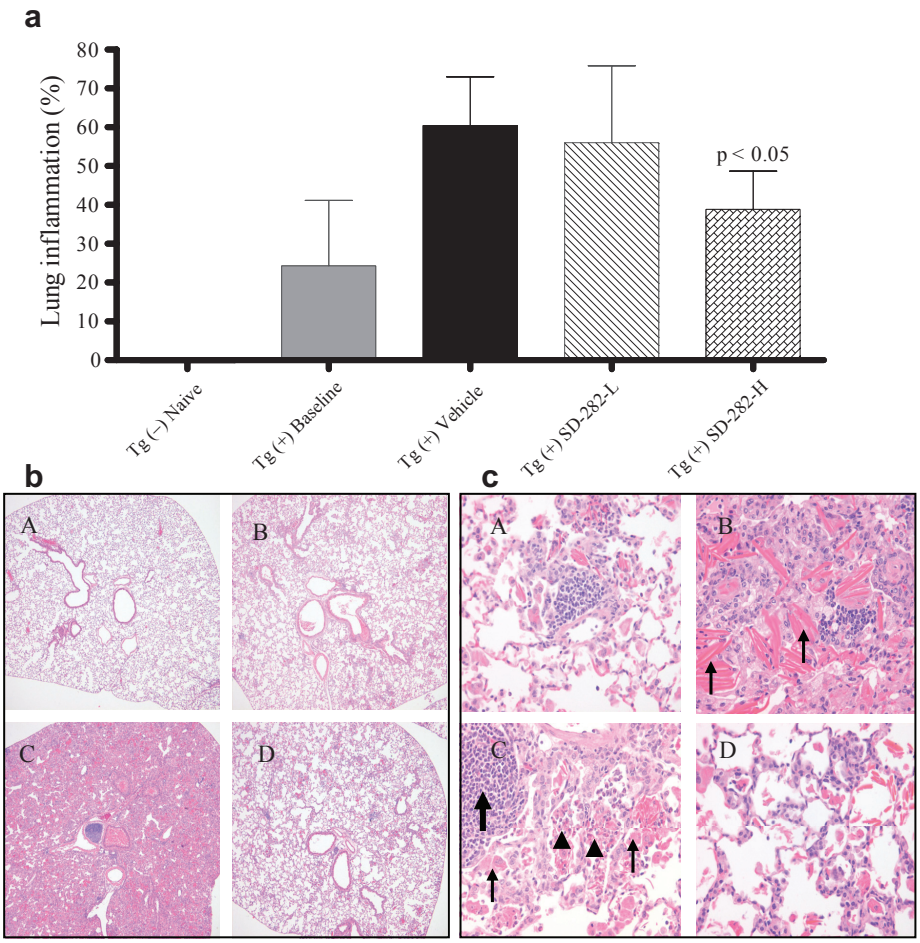

Figure 2 Effect of SD-282 on inflammation induced in the CC10:IL-13 transgenic asthma model analyzed following H&E stain. **[a]** SD-282 at high-dose significantly reduces the inflammation ($p < 0.05$). The noted values represent the MEAN ± SD on a minimum of eight animals. **[b]** SD-282 reduces the inflammatory response. H&E, x40 showing lung sections from Tg (–) naïve (**A**), Tg (+) baseline (**B**), Tg (+) vehicle (**C**) and Tg (+) SD-282H (**D**). **C** showing lungs extremely enlarged and consolidated; alveoli, small and large airway filled with inflammatory cells in the Tg (+) mice treated with vehicle as compared with mild inflammatory response at onset of the asthma (**B**). **D** showing lung with less inflammatory response in SD-282 high-dose treated Tg (+) mice. **[c]** SD-282 reduces crystal formation and prevents eosinophil, lymphocyte, and macrophage infiltration. H&E, x400 showing lung sections from Tg (+) baseline (**A**), Tg (+) vehicle (B and C) and Tg (+) SD-282H (**D**). Mild inflammatory cell infiltration is seen at onset of the asthma/baseline (**A**). Long, thin, rectangular, and needle-like crystals (thin arrow), stained with eosin are seen in the vehicle-treated Tg (+) mice (**B**). Collections of lymphocytes (arrow), eosinophils (arrowhead), and enlarged macrophages (thin arrow) are seen in the vehicle-treated Tg (+) mice (**C**). Reduced crystal formation and fewer eosinophil, lymphocyte, and macrophage are seen in the SD-282 high-dose treated Tg (+) mice (**D**).

low dose showed a trend toward reducing the inflammation but the difference was not significant.

SD-282 reduces hyperplasia of epithelial cell in airway wall

In the Tg (+) baseline group, obvious hyperplasia of bronchial and bronchiolar epithelial cells was observed, with cells being taller and wider compared with the Tg (–) naïve group (Figure 3a and 3b). The thickness of epithelial cells in the segmental bronchus was 0.026 ± 0.004 mm in the baseline group vs 0.016 ± 0.004 mm in the naïve group. In the Tg (+) vehicle-treated group, severe hyperplasia of bronchial and bronchiolar epithelial cells was observed; the thickness of epithelial cells was 0.028 ± 0.004 mm. In the Tg (+) SD-282 high-dose treated group, the thickness of epithelial cells was 0.022 ± 0.003 mm and was reduced to 21% compared with the Tg (+) vehicle group ($p < 0.05$). No improvement of hyperplasia of bronchial and bronchiolar epithelial cells was observed in the SD-282 low-dose group.

SD-282 reduces goblet cell metaplasia and mucus hypersecretion

In normal mice, goblet cells typically comprise less than 20% of cells in the bronchial epithelium, and goblet cell

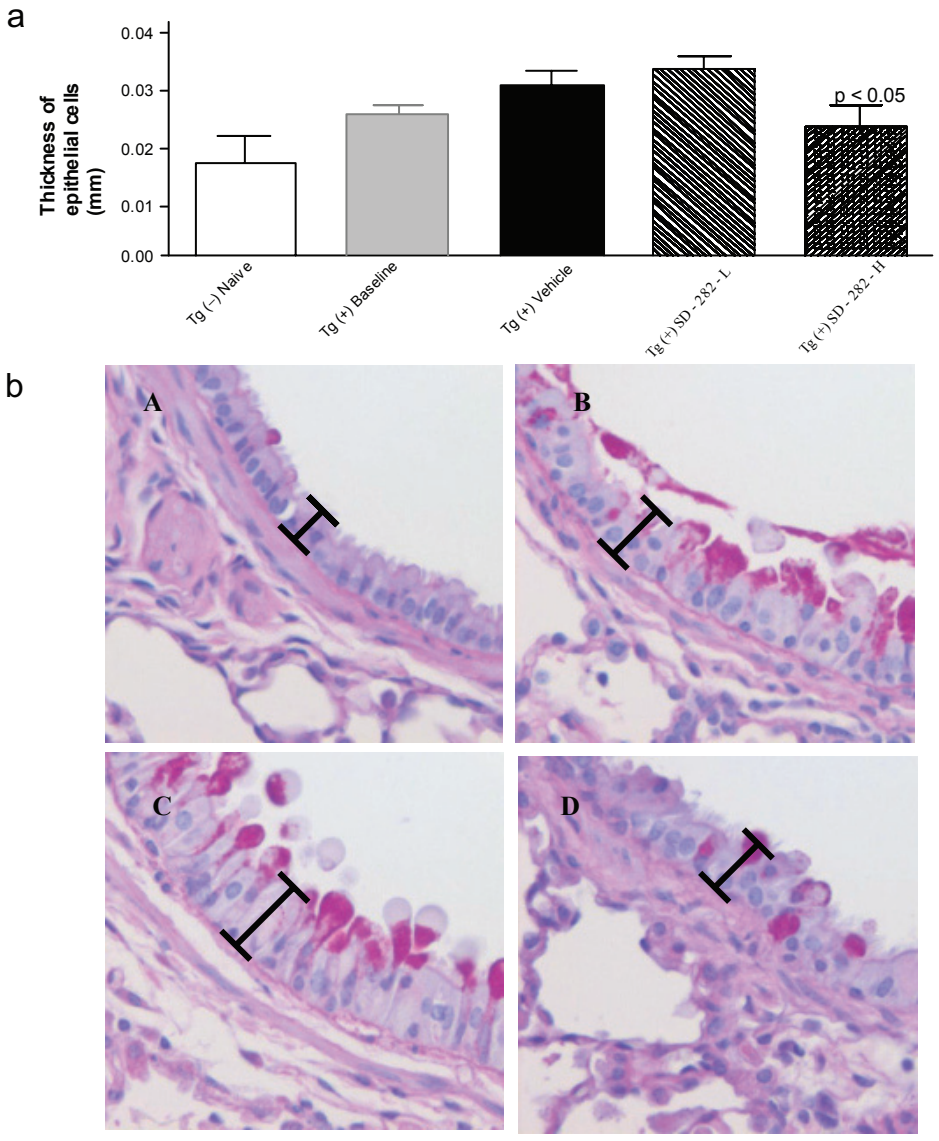

Figure 3 Effect of SD-282 on the hyperplasia of airway wall epithelial cells induced in the CC10:IL-13 transgenic asthma model and analyzed following PASH stain. **[a]** SD-282 at a high-dose significantly reduces the thickness of epithelial cells ($p < 0.05$). The noted values represent the MEAN ± SD on a minimum of eight animals. **[b]** PASH staining of lung sections, ×400 from Tg (–) naïve (**A**), Tg (+) baseline (**B**), Tg (+) vehicle(**C**), and Tg (+) SD-282H (**D**). Increased thickness of epithelial cells is seen in both baseline (**B**) and vehicle-treated Tg (+) mice (**C**) compared with Tg (–) mice (**A**), and decreased thickness of epithelial cells is seen in the SD-282 high-dose treated Tg (+) mice (**D**).

numbers were greatly diminished in the segmental bronchus (Figure 4a, 4b, and 4c). In Tg (+) mice we observed an increased number of goblet cells in the segmental bronchus, and prominent mucus production by airway epithelium in both Tg (+) baseline and Tg (+) vehicle groups. Both neutral (PAS positive) and acidic (Alcin blue positive) mucus were identified (Figure 4b). In the Tg (+) SD-282 high-dose treated group, goblet cell metaplasia and mucin hypersecretion were dramatically inhibited. The percentage of mucin-secreted goblet cells in the segmental bronchus was 22.8% ± 12.11% vs 50% ± 5.8% in the Tg (+) vehicle group, and was reduced by 44% ($p < 0.001$). The inhibition of goblet cell metaplasia and mucus hypersecretion was not observed in the SD-282 low-dose group.

SD-282 reduces subepithelial fibrosis in airway wall

Measurement of thickness of the basement membrane revealed 'thickening' in the membrane (Figure 5a, 5b, and 5c). The 'thickening' was the result of a dense fibrotic response characterized by enhanced accumulation of collagens. We observed very mild collagen deposition around the basement membrane in the Tg (+) baseline group. Enhanced accumulation of collagen was observed in the Tg (+) vehicle group. Significantly less thickening in the basement membrane and subepithelial fibrosis was observed in the SD-282 high-dose group ($p < 0.05$). SD-282 at low dose had no effect on thickening in the basement membrane.

SD-282 reduces fibrosis of lung parenchyma

There was mild remodeling at 8 weeks and obvious organization and remodeling at 12 weeks in the Tg (+) compared to vehicle-treated groups (Figure 5b and 5c). Fibrotic beads with elongated fibroblasts and collagen deposition in the alveolar walls and within the alveoli were observed in the treated groups. The fibrotic changes were very mild in the Tg (+) baseline group. The fibrosis was reduced to 54% in the Tg (+) SD-282 high-dose group ($p < 0.01$).

SD-282 alleviates the severity of asthma

An integrated evaluation of severity of asthma-like histological changes was obtained from the total scores of six histological parameters. The severity of asthma in the transgenic model was significantly reduced to 42% in the Tg (+) SD-282 high-dose group ($p < 0.05$, data not shown).

SD-282 reduces p-p38 MAPK in the lungs

p-p38 MAPK activation was found in bronchial and bronchiolar epithelial cells and infiltrated lymphocytes in the Tg (+) baseline group (Table 1 and Figure 6-1). Enhanced p-p38 MAPK activation was found in Tg (+) vehicle-treated groups. p-p38 activation was found in only one animal in the Tg (+) SD- 282 high-dose group and the activation was inhibited by 25 fold ($p < 0.001$). No p-p38 MAPK activation was found in the Tg (–) naïve group.

SD-282 reduces IL-1β in the lungs

IL-1β expression was found in the inflammatory PMN cells in the lung in the Tg (+) baseline group and enhanced expression of IL-1β was found in the Tg (+) vehicle group (Table 1 and Figure 6-2). The expression was reduced by 3.9-fold in the Tg (+) SD-282 high-dose group ($p < 0.05$).

SD-282 reduces CD3 in the lungs

CD3-positive T lymphocytes, a hallmark and F4/80 positive macrophages numbers, were markedly increased in number in the Tg (+) vehicle-treated group. Both were markedly decreased in number ($p < 0.05$ and $p < 0.01$, respectively) in the Tg (+) SD-282 high-dose treated group (Table 1 and Figure 6-3) and F4/8 IHC (Table 1 and Figure 6-4).

SD-208 reduces fibrosis

Unlike p38 MAPK inhibitor SD-282, TGFβRIK inhibitor SD-208 reduced fibrosis selectively, with no significant effect on lung inflammation. The anti-fibrotic effect is consistent with reduced levels of p-SMAD2/3 (Table 2).

Discussion

IL-13 is a critical cytokine produced largely by activated $CD4^+$ Th2 lymphocytes. Th2-dominated inflammation is a cornerstone of the asthmatic diathesis. The targeted pulmonary expression of IL-13 causes human-like asthma which is characterized by the presence of severe inflammation, edema, and crystal formation in the lung; severe hyperplasia of bronchial and bronchiolar epithelium; marked goblet cell metaplasia and mucus hypersecretion; and moderate fibrosis of airway and lung parenchyma. The CC10-driven overexpression of IL-13 transgenic modeling has also proved to be a powerful method for defining and comparing the in vivo effector functions in asthma-relevant molecules. We used a potent and highly selective p38α-selective MAPK[2] inhibitor, which inhibits kinase activity of the p38 MAPK isoform, to probe the role of p38 MAPK in a CC10:IL-13-driven mouse model of asthma.

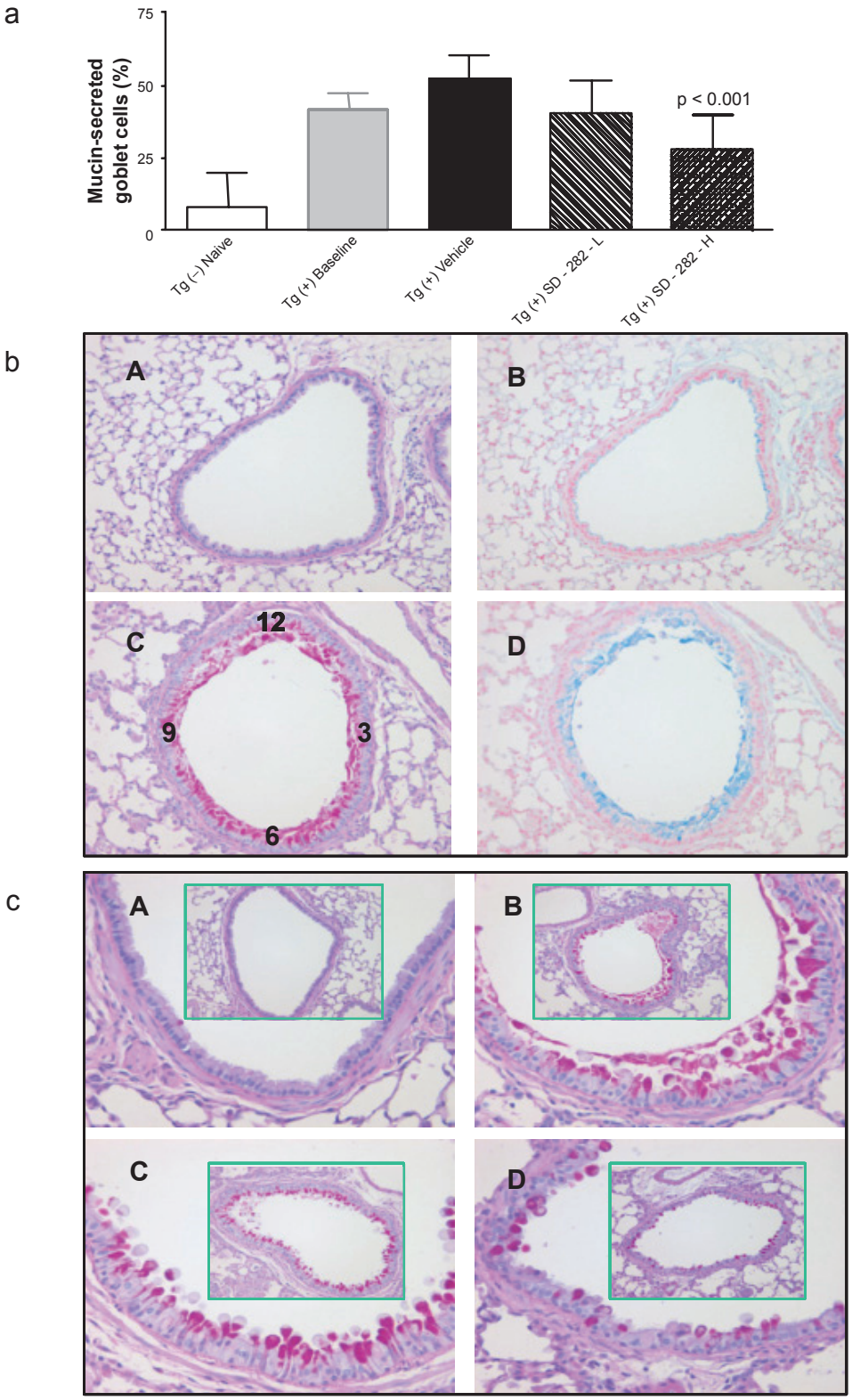

Figure 4 Effect of SD-282 on goblet cell metaplasia and mucus hypersecretion induced in the CC10:IL-13 transgenic asthma model, analyzed after PASH stain. **[a]** SD-282 at a high-dose significantly inhibited the goblet cell metaplasia and mucus hypersecretion ($p < 0.001$). The noted values represent the MEAN ± SD on a minimum of eight animals. **[b]** Neutral and acidic mucus are overproduced in goblet cells of segmental bronchus. PASH and Alcian blue stain, x200 showing lung sections from Tg (–) naïve (**A&B**) and Tg (+) baseline (**C&D**). PASH showing the red-purple cytoplasmic inclusion (neutral mucus) and Alcian blue showing the blue cytoplasmic inclusion (acid mucus). There is almost no neutral and acid mucus production in the epithelial cell in Tg (–) mice (**A&B**). In contrast, there is hypersecretion of both neutral and acid mucus from goblet cells in Tg (+) mice from baseline (**C&D**). **[c]** PASH, x200 (in green box) and x400 showing lung sections from Tg (–) naïve (A), Tg (+) baseline (**B**), Tg (+) vehicle (**C**) and Tg (+) SD-282H (**D**). Mucus overproduction and goblet cell metaplasia are seen in both baseline (**B**) and vehicle-treated Tg (+) mice (**C**) compared with Tg (–) mice (**A**), and decreased mucus production and fewer goblet cells are seen in the SD-282 high-dose treated Tg (+) mice (**D**).

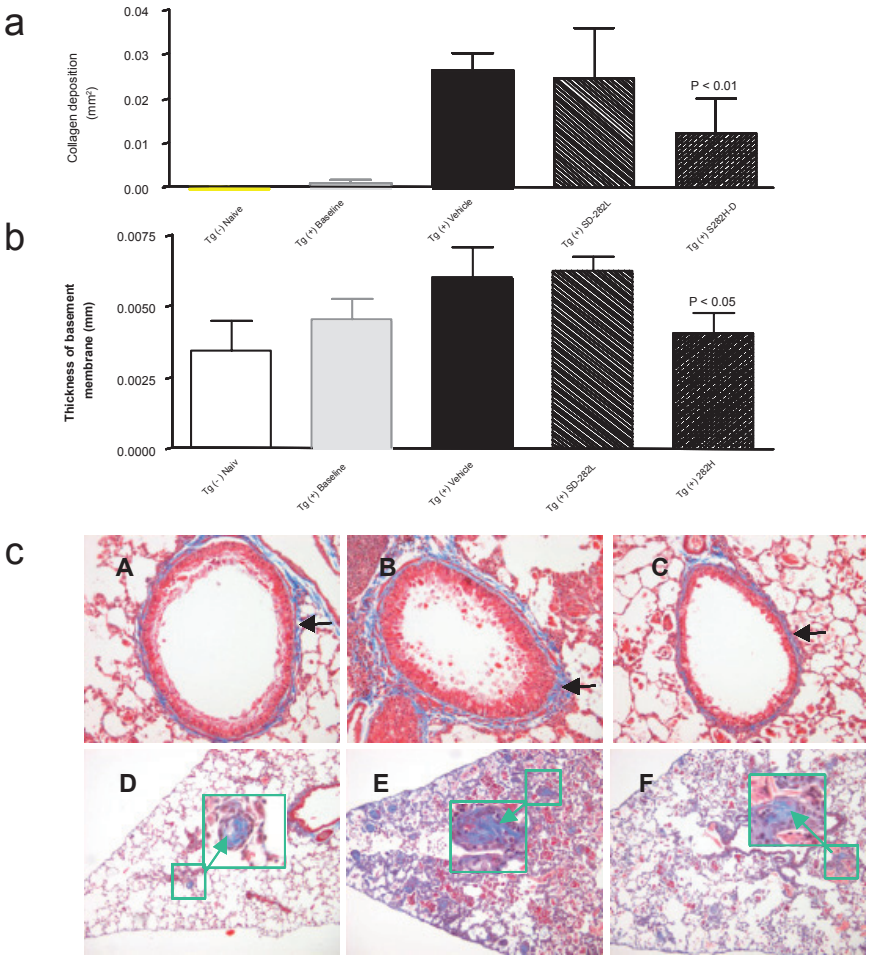

Figure 5 Effect of SD-282 on fibrosis induced in the CC10:IL-13 transgenic asthma model analyzed after Masson's trichrome stain. **[a]** SD-282 at high-dose significantly reduces fibrosis of lung parenchyma compared with the vehicle-treated group ($p < 0.01$). The noted values represent the MEAN ± SD on a minimum of eight animals. [b] Thickness of basement membrane following Masson's trichrome stain. SD-282 at high-dose significantly reduces subepithelial fibrosis compared with the vehicle-treated group ($p < 0.05$). The noted values represent the MEAN ± SD on a minimum of eight animals. **[c]** Masson's trichrome stain, x200 showing lung sections from Tg (+) baseline (**A**), Tg (+) vehicle (**B**) and Tg (+) SD-282H (**C**). Very mild collagen deposition stained in blue (black arrow) around the basement is seen in Tg (+) mice in baseline (**A**). Enhanced accumulation of collagen stained in blue (black arrow) is seen in the vehicle-treated Tg (+) mice (**B**). Less collagen accumulation and reduced thickening in the basement membrane (black arrow) are seen in the SD-282 high-dose treated Tg (+) mice (**C**). Masson's trichrome stain, x100 and x400 (in large green box with arrow) showing lung sections from Tg (+) baseline (**D**), Tg (+) vehicle (**E**), and Tg (+) SD-282H (**F**). Mild fibrotic change is seen in the Tg (+) mice in baseline (**D**). Numerous fibrotic beads with collagen deposition stained in blue (green box) and elongated fibroblasts are seen in the vehicle-treated Tg (+) mice (**E**). Reduced fibrotic beads are seen in SD-282 high-dose treated Tg (+) mice (**F**).

Table 1 Effect of SD-282 on p38 MAPK activation in the airway epithelial cells and infiltrated lymphocytes (analyzed after p-p38 MAPK IHC staining); on IL-1β expression in the inflammatory PMN cells (analyzed after IL-1β IHC staining); on number of infiltrated $CD3^+$ T-lymphocytes (analyzed after CD3 IHC staining), and on activated macrophages in the parenchyma of the lung (analyzed after F4/80 IHC staining) in the CC10:IL13 transgenic mouse asthma model. SD-282 at a high-dose significantly inhibits the level of phosphorylated p38 MAPK in the epithelial cells of airway and infiltrated lymphocytes compared with the vehicle-treated group ($p < 0.001$). SD-282 at a high-dose significantly inhibits IL-1β expression compared with the vehicle-treated group ($p < 0.05$). SD-282 at a high-dose significantly decreases the number of $CD3^+$ T-lymphocytes compared with the vehicle-treated group ($p < 0.05$). SD-282 at a high-dose significantly decreases the number of activated macrophages in the parenchyma of the lung compared with the vehicle group ($p < 0.001$). The noted values represent the MEAN ± SD on a minimum of eight animals. *Values represent scores on the intensity of the IHC staining and #values represent the number of IHC positively labeled cells

Genotype	Treatment	*p-p38 MAPK	*IL-1β	#CD3	#F4/80
Tg (–)	naive	0 ± 0	0 ± 0	64 ± 17	29 ± 8
Tg (+)	baseline	2.13 ± 0.99	1.5 ± 0.53	142 ± 54	110 ± 29
Tg (+)	vehicle	3.3 ± 0.67	2.6 ± 1.07	382 ± 210	183 ± 42
Tg (+)	SD-282	0.13 ± 0.35	0.75 ± 1.04	196 ± 117	92 ± 18
p value		$p < 0.001$	$p < 0.05$	$p < 0.05$	$p < 0.001$

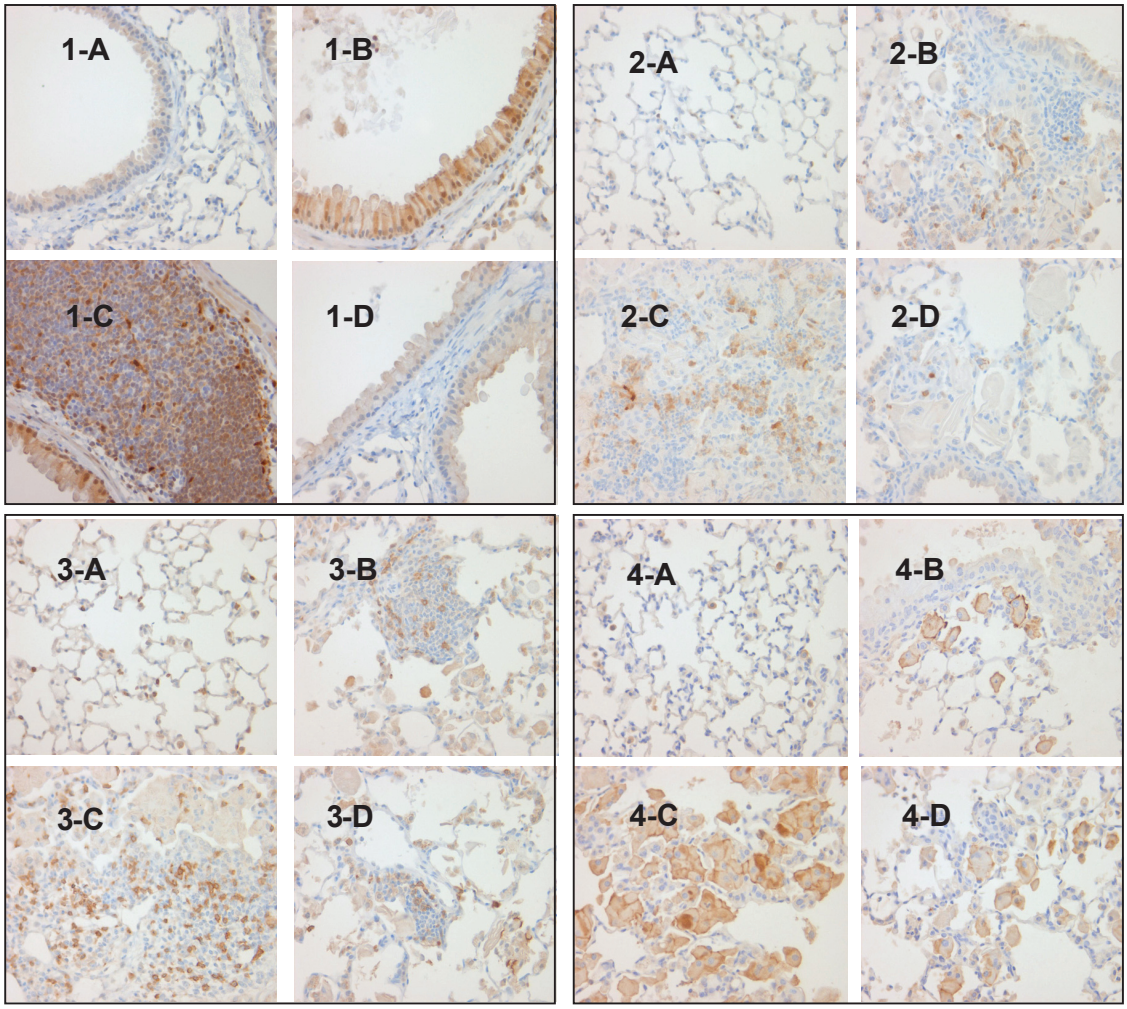

Figure 6 Effect of p38 MAPK inhibition on immune cell infiltration and activation in CC10:IL-13 mice **[1]** p-p38 MAPK IHC stain, x400 showing no p-p38 MAPK activation in Tg (–) mice (**1-A**), enhanced p-p38 MAPK activation in the epithelial cells of airway (**1-B**) and infiltrated lymphocytes(**1-C**) in the vehicle-treated Tg (+) mice and completed inhibition of p-p38 MAPK activation in the epithelial cells in the SD-282 high-dose treated Tg (+) mice (**1-D**). **[2]** IL-1β IHC stain, x400 showing no IL-1β expression in Tg (–) mice (**2-A**), mild IL-1β expression in the PMN cells in Tg (+) mice in baseline (**2-B**), increased IL-1β expression in the vehicle-treated Tg (+) mice (**2-C**) and less IL-1β expression in the PMN cells in the SD-282 high-dose treated Tg (+) mice (**2-D**). **[3]** CD3 IHC stain, x400 showing few $CD3^+$T-lymphocytes in the lung of Tg (–) mice (**3-A**), mild $CD3^+$ T-lymphocyte infiltration in the lung of Tg (+) mice in baseline (**3-B**), markedly increased number of $CD3^+$ T-lymphocyte in the lung of Tg (+) mice treated with vehicle (**3-C**) and significantly decreased number of $CD3^+$ T-lymphocytes in the lung of Tg (+) mice treated with the high-dose of SD-282 (**3-D**). **[4]** F4/80 IHC, x400 showing no activated macrophages in the lung of Tg (–) mice (**4-A**), few activated macrophages in the lung of Tg (+) mice in baseline (**4-B**), markedly increased number of activated macrophages in the lung of Tg (+) mice treated with vehicle (**4-C**), and decreased number of activated macrophages in the lung of Tg (+) mice treated with high-dose of SD-282 (**4-D**).

Our present findings reveal that p38 MAPK phosphorylation, shown IHC assay in the lung tissue of transgenic mice, was significantly higher compared with non-transgenic naïve mice. SD-282 at high-dose (90 mg/kg twice daily) produces inhibition of the p38 MAPK activation in the epithelial cells of the airway and in the infiltrating lymphocytes, and attenuates IL-13-induced pulmonary inflammation, release of Th2 cytokines into the airway, airway mucus production, hyperplasia of airway epithelium and lung fibrosis. This finding proves that p38 MAPK plays an important roll in CC10: IL-13 asthma.

Our data show that the p38α-selective MAPK inhibitor significantly reduces the number of $CD3^+$ T-cells and macrophages in the lung. There is now clear evidence that Th2 cells play an essential role in the pathogenesis of asthmatic airway inflammation (Herrick et al 2003; Larche et al 2002). Th2 cytokines can be produced by various resident cells, including bronchial epithelial cells, tissue mast cells, and alveolar macrophages, and by infiltrating inflammatory cells, such as lymphocytes and eosinophils. The p38 MAPK signaling pathway has been shown to be involved in cytokine production from

Table 2 Effect of TGFβRI kinase inhibitor, SD-208 and p38α-selective MAPK inhibitor, SD-282 both at a high-dose significantly reduce fibrosis of lung parenchyma compared with the vehicle-treated group ($p < 0.05$ and $p < 0.01$). The noted values represent the MEAN ± SD on a minimum of eight animals

Genotype	Treatment	Fibrosis of lung parenchyma mm^2/per section	p value
Tg (–)	naive	0 ± 0	
Tg (+)	baseline	0.00098 ± 0.00059	
Tg (+)	vehicle	0.02631 ± 0.01210	
Tg (+)	SD-208	0.01629 ± 0.0038	$p < 0.05$
Tg (+)	SD-282	0.01213 ± 0.0077	$p < 0.01$

a variety of cell types. TCR engagement and/or CD28 co-stimulation of $CD4^+$ T cells has been shown to induce IL-4 and IL-13 production and Th2 cell differentiation via activation of p38 MAPK (Schafer et al 1999; Skapenko et al 2001; Lu et al 2004).

Eosinophils, lymphocytes, and macrophages are believed to be the principal effector cells for the pathogenesis of inflammation of asthma. Our present findings show that the administration of the p38α-selective MAPK inhibitor prevents eosinophil and lymphocytes infiltration into the airways and reduces the number of macrophages. Similarly, IHC assay also confirmed that the p38α-selective MAPK inhibitor reduces the number of $CD3^+$ T-lymphocytes and F4/80 macrophages. Eosinophil transmigration into the airways is a multi-step process, orchestrated by Th2 cytokines such as IL-4, IL-5, and IL-13, and coordinated by specific chemokines in combination with adhesion molecules, such as vascular cell adhesion molecule-1 (VCAM-1) and very late antigen-4 (VLA-4) (Lukacs et al 2001; Koo et al 2003). IL-13 has been shown to be by far the most potent inducer of eotaxin expression by airway epithelial cells (Li et al 1999). Furthermore, the p38 MAPK pathway has been shown to be involved in the intrinsic mechanism of eotaxin-induced eosinophil cytoskeletal rearrangements, chemotaxis, and degranulation (Kampen et al 2000); together the observed reduction in airway eosinophilia by the p38α-selective MAPK inhibitor is likely a result of reduction in Th2 cytokine production, leading to downregulation of chemokine production and eosinophil chemotaxis.

Our findings demonstrate a dramatic reduction in mucus production with less goblet cell hyperplasia in the Tg (+) SD-282 high-dose treated group compared with the Tg (+) vehicle-treated group. Studies using undifferentiated tracheobronchial epithelial cells showed that Th2 cells and cytokines (Zhu et al 1999; Justice et al 2002) are linked to mucus hypersecretion by their effects on mucin gene expression in the airway epithelium. In addition, a recent study showed that IL-13-induced goblet cell hyperplasia, and mucin MUC5AC protein expression in human bronchial epithelial cell cultures, were mediated by the p38 MAPK signaling pathway and could be inhibited by a p38 inhibitor (Atherton et al 2003). Therefore, the observed decrease in mucus production in the p38α-selective MAPK inhibitor treated group may be attributed to the substantial drop in Th2 cytokines in asthmatic mice treated with vehicle and/or downregulation of p38α-selective MAPK in the IL-13 responsive airway epithelium.

It is well-established that p38 MAPK regulates key pro-inflammatory molecules in inflammatory cells (Schafer et al 1999; Nath et al 2006). Our findings demonstrate that IL-1β expression was significantly inhibited by SD-282 in inflammatory PMN cells. The down regulation of IL-1β by SD-282 supports inhibition of p-38 related IL-1β release from the inflammatory cells.

The stimuli that induce airway remodeling are not well defined. This is compounded by the complex relationship between inflammation and remodeling, with chronic inflammation inducing remodeling responses in some settings. The relationship between inflammation and remodeling gains support from the results reported here. We observed mild fibrosis in the early stage and severe fibrosis in the late stage of asthma development in mice. Our finding demonstrate that fibrosis was significantly reduced in the Tg (+) SD-282 high-dose treated group compared with the Tg (+) vehicle-treated group. The MAPK and TGFβR1/SMAD2/3 signaling pathways play critical roles in inflammation and fibrogenesis, respectively (Li et al 2006). It is very well established that the MAPK pathway is responsive to TGFβR1 stimulation and coordinates with SMAD2/3 signaling in many inflammatory and fibrotic disease states (Kapoun et al 2006; Dziembowska et al 2007; Martin et al 2007). Inflammation and fibrogenesis are the two determinants of the

progression of lung fibrosis, the common pathway leading to end-stage lung disease (Li et al 2006). In the lungs of CC10: IL-13 transgenic mice, both phosporylated p38 MAPK and SMAD2/3 are upregulated. Whereas p38 MAPK is activated in the early stage of lung disease, SMAD2/3 activation is seen at the end stage of the disease. This temporal separation may reflect differing roles in the natural history of lung pathology, with p38 MAP kinase acting as a central mediator in an early inflammatory phase, and TGFβRI kinase acting as a central mediator of firosis in a late resolution phase. Differentiation of these processes can be seen in our data, showing that p38α-selective MAPK inhibitor, SD-282 attenuated both inflammation and fibrosis whereas TGFβRI inhibitor, SD-208 selectively reduced fibrosis. The pivotal roles of p38α-selective MAPK inhibitor in reducing inflammation and TGFβRI inhibitor in reducing fibrosis are clearly in agreement with our previous report profiling the effects in lung fibroblasts (Kapoun et al 2006). The additional role of p38α-selective MAPK, SD-282 in reducing fibrosis is a novel finding and may relate to the documented cross talk between the p38 MAPK and TGFβRIK pathways (Martin et al 2007; Dziembowska et al 2007). SD-282 reduced inflammation, possibly via directly inhibiting p38 MAPK activation in lymphocytes, and reduces hyperplasia of airway epithelium and goblet cell metaplasia, possibly via directly inhibiting p38 MAPK activation in the airway epithelial. Therefore SD-282 indirectly reduced lung remodeling and fibrosis induced by chronic inflammation. Our data are in agreement with observations of Ross and his colleagues (Ross et al 2006) in which SMAD2/3 expression is regulated by MAPK kinase-1 in epithelial and smooth muscle cells.

In summary, we have shown in the CC10:IL-13 mouse model of asthma that p38α-selective MAPK inhibitor SD-282 at a high-dose of 90 mg/kg (twice/per day, orally) given as therapeutic treatment at the onset of asthma for a period of four weeks, directly reduces inflammation, hyperplasia of airway epithelium, goblet cell metaplasia, and mucus hypersecretion. In contrast to directly reducing fibrosis with TGFβRI inhibition, p38 MAPK inhibition indirectly reduces the lung remodeling and fibrosis and consequently alleviates the severity of lung damage. This study provides evidence that p38α-selective MAPK inhibitor may play a dual role in attenuating both inflammation and fibrosis in asthma. Inhibition of this enzyme may be have therapeutic potential for asthma and other Th2-polarized inflammatory lung diseases.

Disclosure

The authors report no conflicts of interest in this work.

References

Atherton HC, Jones G, Danahay H. 2003. IL-13-induced changes in the goblet cell density of human bronchial epithelial cell cultures: MAP kinase and phosphatidylinositol 3-kinase regulation. *Am J Physiol Lung Cell Mol Physiol*, 285:L730–L9.

Dziembowska M, Danikiewicz M, Wesolowska A, et al. 2007. Cross-talk between Smad and p38 MAPK signaling in transforming growth factor beta signal transuction in human blioblastoma cells. *Biochem Biophys Res Commun*, 354; 1101–6.

Gupta PK. 1998. Pulmonary cytopathology. In: Fishman AP, et al. (eds). *Fishman's pulmonary diseases and disorders.* 3rd ed. New York, NY: McGraw-Hill, pp. 487–504.

Herrick CA, Bottomly K. 2003. To respond or not to respond: T cells in allergic asthma. *Nat Rev Immunol*, 3:1–8.

Hogan B, Constantini F, Lacy E. 1986. *Manipulating the mouse embryo: a laboratory manual.* Cold Spring Harbor, NY: Cold Spring Harbor Laboratory Press, pp. 1–332.

Jiang Y. Gram H, Zhao M, et al. 1997. Characterization of the structure and function of the fourth member of p38 group mitogen-activated protein kinase, p38 δ. *J Biol Chem*, 272:30112–28.

Justice JP, Crosby J, Borchers MT, et al. 2002. $CD4^+$ T cell-dependent airway mucus production occurs in response to IL-5 expression in lung. *Am J Physiol Lung Cell Mol Physiol*, 282:L1066–74.

Kampen GT, Stafford S, Adachi T, et al. 2000. Eotaxin induces degranulation and chemotaxis of eosinophils through the activation of ERK2 and p38 mitogen-activated protein kinases. *Blood*, 95:1911–7.

Kapoun AM, Gaspar NJ, Wang Y, et al. 2006. Transforming growth factor-beta receptor type 1 (TGFbetaR1) kinase activity but not p38 activation is required for TGFbetaR1-induced myofibroblast differentiation and profibrotic gene expression. *Mol Pharmacol*, 70:518–31.

Koo GC, Shah K, Ding GJF, et al. 2003. A small molecule very late antigen-4 antagonist can inhibit ovalbumin-induced lung inflammation. *Am J Respir Crit Care Med*, 167:1400–9.

Larche MD, Robinson S, Kay AB. 2002. The role of T lymphocytes in the pathogenesis of asthma. *J Allergy Clin Immunol*, 111:450–63.

Li J, Campanale NV, Liang RJ, et al. 2006. Inhibition of p38 mitogen-activated protein kinase and transforming growth factor-beta1/Smad signling pathways modulates the development of fibrosis in adriamycin induced nepropathy. *Am J Pathol*, 169:1527–40.

Li L, Xia Y, Nguyen A, et al. 1999. Effects of Th2 cytokines on chemokine expression in the lung: IL-13 potently induces eotaxin expression by airway epithelial cells. *J Immunol*, 162:2477–87.

Lu B, Ferrandino AF, Flavell RA. 2004. Gadd45ß is important for perpetuating cognate and inflammatory signals in T cells. *Nat Immunol*, 5:38–44.

Lukacs NW. 2001. Role of chemokines in the pathogenesis of asthma. *Nat Rev Immunol* 1:108–16.

Martin MM, Buckenberger JA, Jiang J, et al. 2007. TGF-beta stimulates human AT1 receptor expressiion in lung fibroblasts by cross talk between the Smad, p38 MAPK, JNK, and PI3K isignaling pathways. *Am J Physiol Lung Cell Mol Physiology*, 293:790–9.

Medicherla S, Ma JY, Mangadu R, et al. 2006. Selective p38{alpha} Mitogen-activated protein kinase inhibitor reverses cartilage and bone destruction in mice with collagen-induced arthritis. *J Pharmacol Exp Ther*, 318:132–41.

Nath P, Leung SY, Williams A, et al. 2006. Importance of p38 mitogen-activated protein kinase pathway in allergic airway remodelling and bronchial hyperresponsiveness. *Eur J Pharmacol*, 544(1–3):160–7.

Pack RJ, Al-Ugaily LH, Morris G. 1981. The cells of the tracheo- bronchial epithelium of the mouse: a quantitative light and electron microscope study. *J Anat*, 132:71–84.

Ray P, Tang W, Wang P, et al. 1997. Regulated overexpression of interleukin-11 in the lung: use to dissociate development-dependent and -independent phenotypes. *J Clin Invest*, 100:2501–11.

Ross KR, Corey DA, Dunn JM et al. 2006. SMAD3 expression is regulated by mitogen-activated protein kinase kinase-1 in epithelial and smotth muscles cells. *Cell Signal*, 19:923–31.

Schafer PH, Wadsworth SA, Wang L, et al. 1999. p38 α mitogen-activated protein kinase is activated by CD28-mediated signaling and is required for IL-4 production by human $CD4^+CD45RO^+$ T cells and Th2 effector cells. *J Immunol*, 162:7110–9.

Skapenko A, Lipsky PE, Kraetsch HG, et al. 2001. Antigen-independent Th2 cell differentiation by stimulation of CD28: regulation via IL-4 gene expression and mitogen-activated protein kinase activation. *J Immunol*, 166:4283–92.

Sugden PH, Cleark A. 1998. "Stress-responsive" mitogen-activated protein kinases (c-Jun N-terminal kinases and p38 MAPK mitogen-activated protein kinases) in the myocardium. *Circ Res*, 83:345–52.

Sweitzer SM, Medicherla S, Almirez R, et al. 2004. Antinociceptive action of a p38 alpha MAPK inhibitor, SD-282, in a diabetic neuropathy model. *Pain*, 109:409–19.

Tang W, Geba GP, Zheng T, et al. 1996. Targeted expression of IL-11 in the murine airway causes airways obstruction, bronchial remodeling and lymphocytic inflammation. *J Clin Invest*, 98:2845–53.

Underwood DC, Obsorn RR, Kotzer CJ, et al. 2000. SB 239063, a potent p38 MAPK kinase inhibitor, reduces inflammatory cytokine production, airways eosinophil infiltration, and persistence. *J Pharmacol Exp Ther*, 293:281–8.

Zhu Z, Homer RJ, Wang Z, et al. 1999. Pulmonary expression of interleukin-13 causes inflammation, mucus hypersecretion, subepithelial fibrosis, physiologic abnormalities, and eotaxin production. *J Clin Invest*, 103:779–88.